Biophysical Journal

Supporting Material

Torsional Behavior of Axonal Microtubule Bundles

Carole Lazarus,[1] Mohammad Soheilypour,[1] and Mohammad R. K. Mofrad[1,*]

[1]Molecular Cell Biomechanics Laboratory, Departments of Bioengineering and Mechanical Engineering, University of California, Berkeley, California

SUPPORTING MATERIAL

A. Parameters of simulation

Table 1: Modeling parameters (1, 2)

Parameter	Value
MT Young's modulus, E_{MT}	1.5 GPa
MT flexural rigidity, EI_{MT}	1.8 10^{-24} Nm^2
MAP tau protein Young's modulus, E_{CL}	5.0 MPa
MT element length, l_0^{MT}	10 nm
MAP tau protein element length, l_0^{CL}	45 nm
MT axial spring constant, k_s^{MT}	47.1 N/m
MT bending spring constant, k_b^{MT}	1.8 10^{-16} Nm
MAP tau protein axial spring constant, k_s^{CL}	3.925 10^{-2} N/m
MT bead mass, m_{MT}	1.48375 10^{-21} kg
MAP tau protein bead mass, m_{CL}	2.0 10^{-22} kg
Microtubule resistance coefficients, C_n^{MT}, C_t^{MT}	2.1191, 1.2700
MAP tau protein resistance coefficients, C_n^{CL}, C_t^{CL}	5.9555, 4.9181
Time step, δt	0.1 ps
Steric energy scaling parameter ϵ_0	1.10^{-16} Nm
Steric radius, σ_0	12.5 nm

B. Discrete bead-spring model

MT beads are connected by linear springs with potential V_s given by the equation:

$$V_s = k_s \frac{(|\mathbf{r}| - l_0)^2}{2} \tag{1}$$

where k_s is the spring constant, $\mathbf{r}$ is the separation distance, and l_0 is the unstretched length of the spring. The spring constant is related to the material properties of the filament by the equation,

$$k_s = \frac{EA}{l_0} \tag{2}$$

where E is the Young's modulus of the filament and A is the cross-sectional area of the filament. MAP tau proteins are modeled as two-node linear spring elements, a representation common to a number of cross-linked network models.

The bending potential is represented by a harmonic potential as a function of the bend angle θ. The bending potential V_b thus takes the following form:

$$V_b = k_b \frac{(\theta - \theta_0)^2}{2} \tag{3}$$

where k_b is the bending spring constant, θ is the angle between susbsequent elements, and θ_0 is the rest angle of the bend. The bending spring constant is related to the material properties of the filament by the following equation:

$$k_b = \frac{EA}{I} \tag{4}$$

where EI is the flexural rigidity of the filament. The flexural rigidity of a polymer is related to its persistence length in the equation:

$$EI = l_p k_b T \tag{5}$$

where l_p is the persistence length, k_b is the Boltzmann constant and T the temperature.

Moreover, given the tight packing configuration of the bundle, MTs are likely to penetrate neighboring filaments in the bundle. Therefore it is essential to incorporate a repulsive force to prevent this unrealistic event. This is implemented by adding a regulatory steric repulsion force with an arbitrarily chosen exponentially decaying potential $V_s r$:

$$V_{sr} = \epsilon_0 e^{-\frac{|\mathbf{r}|}{\sigma_0}} \tag{6}$$

where ϵ_0 is the energy scaling parameter, $\mathbf{r}$ is the distance between sterically interacting beads, and σ_0 is the steric radius. The steric radius is set to the outer MT radius, 12.5 nm, and the energy scaling parameter is selected to prevent penetration with minimal long-range effects. A cutoff radius of 2.4 σ_0 is used to truncate the steric interaction for computational efficiency while preventing filament penetration.

The interaction forces are then derived from the potentials using the equation:

$$\mathbf{F}_{ji} = -\nabla V(\mathbf{r}_{ij}) \tag{7}$$

where V is the interaction potential and $\mathbf{r}_{ij}$ is the vector from bead i to bead j.

In our model, the presence of the cytoplasm is represented by tangential and normal drag forces on the MTs and MAP tau proteins with viscosity μ. The MTs and tau proteins resistance coefficients (C^{MT}, C^{CL}) describe the amount of drag force experienced by each of the elements. However, brownian forces are not considered in this model due to the high persistence length of MTs, i.e. 420 μm, and dominance of exterior forces.

C. Application of torsion and calculation of bundle angle

Application of torsion

For small deformations, orthoradial force and associated shear stress are a linear function of radius. Assuming that the 3 radii of the bundle maintain their relative ratio as shown in Eq. 8, the forces can be calculated as in Eq. 9 at each time:

$$R_2 \approx \sqrt{3} R_1 \; ; \; R_3 \approx 2 R_1 \tag{8}$$

$$f_2 = \sqrt{3} f_1 \; ; \; f_3 = 2 f_1 \tag{9}$$

Therefore:

$$f_1 = \frac{T}{48 R_1} \; ; \; f_2 = \frac{R_2}{R_1}\frac{T}{48 R_1} \; ; \; f_3 = \frac{R_3}{R_1}\frac{T}{48 R_1} \tag{10}$$

Finally, the orthoradial forces must be projected in the y- and z-axes, and after applying some simplifications:

$$\begin{aligned} f_{iy} &= -\frac{T}{48 R_{avg}^2} z \\ f_{iz} &= \frac{T}{48 R_{avg}^2} y \end{aligned} \tag{11}$$

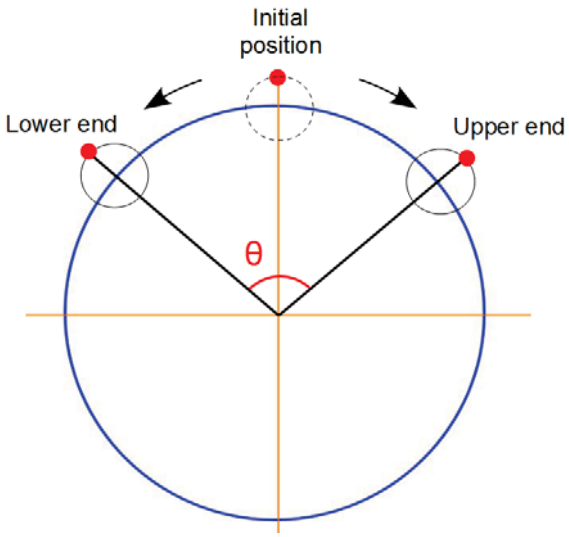

Figure 1: Calculation of bundle angle. Initially both ends of a single MT filament are aligned on the central axis of the bundle. Upon application of torsional loading, the two ends of the filaments move in opposite directions. The angle θ formed by a single filament is calculated as shown in the figure.

Calculation of bundle angle and number of bundle turns

Bundle angle is calculated by averaging the angle formed by each of the twelve external MT filaments with respect to the central axis. The angle made by an individual MT filament can be visualized in Fig. 1.

Assuming that (y_1, z_1) and (y_2, z_2) are the transverse coordinates of the two ends of a single MT filament, the angle can be calculated by Eq. 12:

$$cos(\theta) = \frac{y_1 y_2 + z_1 z_2}{\sqrt{(y_1^2 + z_1^2)(y_2^2 + z_2^2)}} \tag{12}$$

Number of bundle turns is calculated as a function of time in Figure 2. Upon 3 bundle turns, a change of regime from a linear to a non-linear behavior is observed. This strongly suggests a change in mechanical behavior of the MT bundle under torsion at 3 bundle turns.

D. Verification of model assumptions

To verify whether cross-sections remain parallel to each other, we calculated the x-deviation σ_{x0}, i.e. deviation in x-axis, from the initial position as well as the x-deviation between beads of the same cross-section. We monitored this value to make sure that it does not exceed twice of the bead-spacing, i.e. 10 nm.

$$\begin{aligned} \sigma_{x0} &= \frac{\sqrt{\sum (x_i - x_0)^2}}{18} \\ \sigma_x &= \frac{1}{2}\frac{\sqrt{\sum (x_i - x_j)^2}}{18 * 17} \end{aligned} \tag{13}$$

The deviation from the initial hexagonal bundle geometry was also evaluated by calculating the relative error that arises when assuming that the six beads of one of the three initial circles (i=1,2,3) stay in a circle.

$$\sigma_{r_i} = \frac{\sqrt{\frac{1}{5}\sum_{i=1}^{6}(r_i - \overline{r})^2}}{\overline{r}} \tag{14}$$

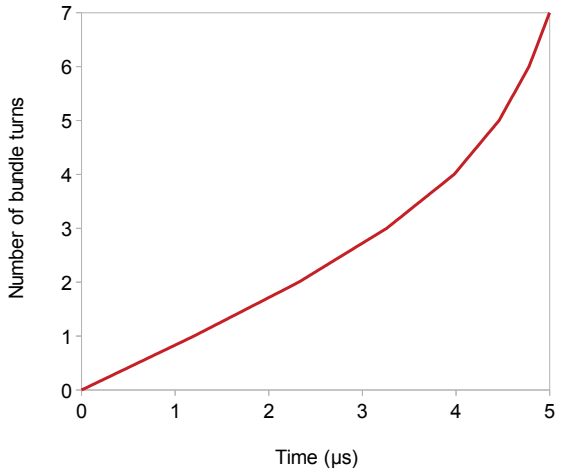

Figure 2: Number of bundle turns as a function of time. Up to 3 turns, a linear increase is observed. From 3 to 7 turns, the number of turns accelerates with time, becoming a non-linear function of time.

These values were calculated for the nine 1 μm-spaced cross-sections and was eventually averaged among all of them.

Figure 3 shows that for the maximum turns studied here, σ_x remains below 20 nm. In addition, the quantity σ_{x0} never exceeds 6 nm, except for the bundle ends where it reaches 10 nm after 7 turns.

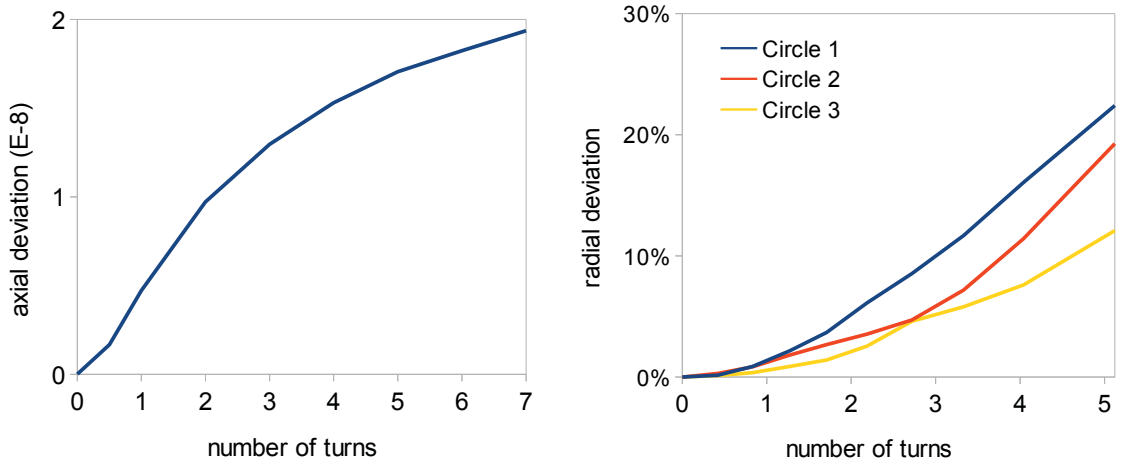

Figure 3: Left: x-deviation σ_x as a function of number of turns. Right: Relative error σ_{r_i} of hexagonal configuration for each circle i.

As far as the preservation of the bundle hexagonal geometry is concerned, one first rough estimation can be done visually (Fig. 4). As we can observe, the hexagonal geometry is preserved for about 3 turns but is eventually deformed by further twisting.

The relative error σ_r shows that hexagonal configuration is relatively maintained in the middle of the bundle. Particularly, the outer circle, which was chosen to calculate the average bundle radius, is stable, reaching a relative error of less than 15% after 5 μs.

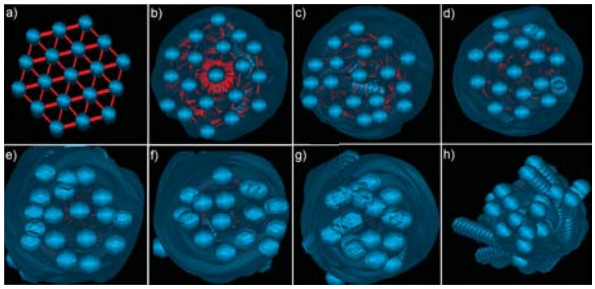

Figure 4: Visualization of initial hexagonal geometry deformation. a) 0 turn ; b) 0.83 turn ; c) 1.7 turns ; d) 2.7 turns ; e) 4 turns ; f) 5.1 turns ; g) 7 turns ; h) more than 8 turns.

E. Energy curves during relaxation

Upon release of torsional loading at 1 μs, a sharp increase in different energies is observed. Curves for MAP tau tensile energy and MT bending energy are displayed in Fig. 5.

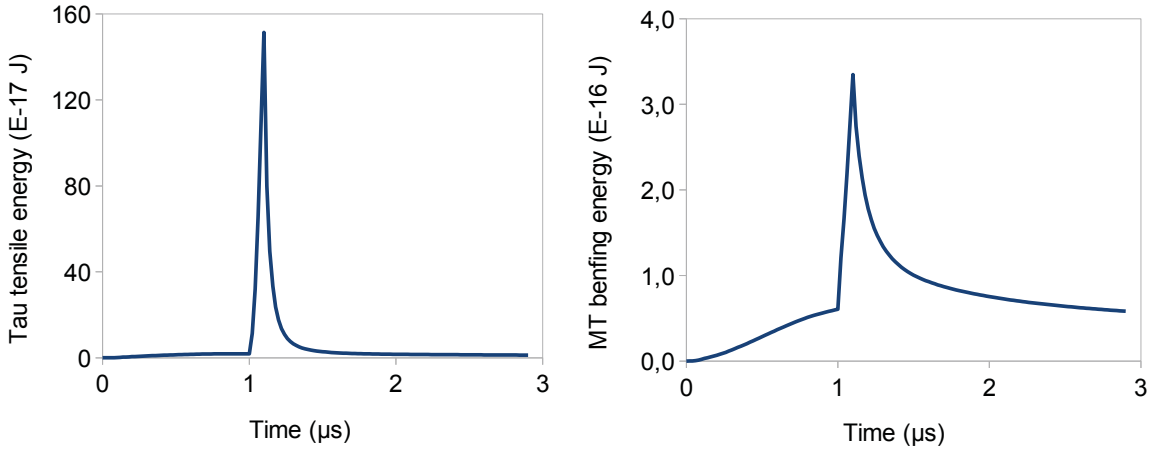

Figure 5: Left: MAP tau tensile energy during relaxation experiment. Sharp increase of approximately 10-folds is observed upon release of torsional loading at 1 μs. Right: MT bending energy during relaxation experiment. A significant increase of approximately 8-folds is observed upon release of torsional loading.

F. Sensitivity Analysis

Since different input parameters were used in our model, a sensitivity analysis is required to make sure the results are reliable. We have previously performed a thorough sensitivity analysis on the model in our first study on mechanical behavior of microtubules under tension (2) Fig. 6. Different parameters, including microtubule bending stiffness, microtubule elastic modulus, MAP tau elastic modulus, and MAP tau length were increased/decreased by 5%, 10%, and 50%. Our results demonstrated that the model is not very sensitive to modest changes in the system parameters, suggesting that the results are acceptable given parameter estimates with reasonable agreement to true physiological values.

Supporting References

[1] Blundell, J. R., E. M. Terentjev. 2009. Stretching semiflexible filaments and their networks. Macromolecules. 42:5388-5394

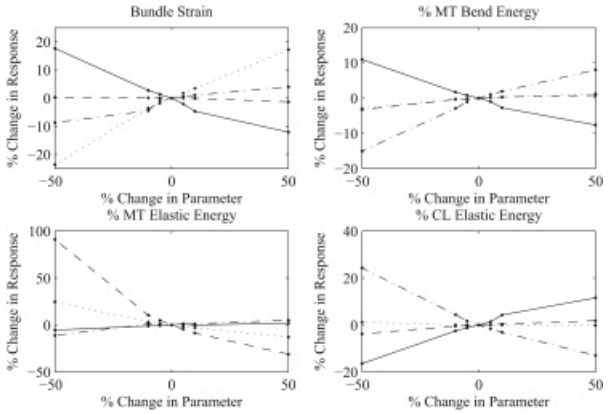

Figure 6: Sensitivity plots of the bundle response to different parameters. Microtubule bending stiffness (solid line), microtubule elastic modulus (dashed line), cross-link elastic modulus (dash dotted line), and cross-link length (dotted line) are varied. Response sensitivity is monitored as the percent change in bundle strain (top left), percentage of energy stored in microtubule bending (top right), percentage of energy stored in microtubule stretching (bottom left), and percentage of energy stored in cross-link stretching (bottom right). The model shows relatively low sensitivity to modest changes in system parameters, lending confidence to the conclusions.

[2] Stephen J. Peter, Mohammad R.K. Mofrad. 2012. Computational Modeling of Axonal Microtubule Bundles under Tension. Biophys. J. 102:749-57.